The Radiometric Characterization of AMSU-B

Roger W. Saunders, Timothy J. Hewison, Stephen J. Stringer, and Nigel C. Atkinson

Abstract—The Advanced Microwave Sounding Unit, AMSU, is being developed to fly on the new generation of NOAA polar orbiters due to be launched in the latter half of the 1990's. The U.K. Meteorological Office (UKMO) are procuring the high frequency component of AMSU (AMSU-B) with five channels in the range 88–191 GHz. In order to determine the radiometric performance and verify the method for calibration of AMSU-B an extensive series of tests have been performed by the UKMO on the engineering and three flight models. The instruments were placed in a 3 m thermal-vacuum chamber where their temperature could be controlled over the full range expected in orbit and an *Earth* target and a *space* target could be viewed. For the first flight model the measured NeΔT values were all <1.1 K at the nominal instrument temperature using a 300 K target. Absolute calibration accuracy and linearity in response were measured to be well within the specification of 1 and 0.3 K, respectively. A small variation in the gain with scan angle was found and an empirical factor was derived to modify the inferred radiances to remove this effect. Measurements of the gain stability for each channel were also measured for simulated in-orbit conditions.

Index Terms—AMSU, microwave radiometer, calibration.

I. INTRODUCTION

THE NEXT MAJOR step forward in temperature and humidity sounding of the atmosphere from space is the introduction of a new generation of microwave radiometers. They will provide improved accuracy in temperature retrievals, especially in the stratosphere, and much improved humidity retrievals especially in the lower troposphere [1]. They will also improve the coverage obtained, by being less affected by cloud cover than the infrared sounders particularly over the extensive sheets of maritime stratocumulus cloud.

The current operational sounder TOVS (TIROS Operational Vertical Sounder), on the NOAA polar orbiting satellites will be upgraded to the ATOVS (Advanced TOVS) system due for launch on NOAA's K, L, and M in the mid 1990's. The new generation of instruments which will make up the ATOVS are an infrared sounder, HIRS-3, (similar to the previous version) and a new 20-channel Advanced Microwave Sounding Unit (AMSU). AMSU is comprised of three separate instruments: AMSU-A1 and AMSU-A2, which have the 15 lower frequency channels (23.8–89.0 GHz) primarily for temperature sounding (surface to 2 hPa), and AMSU-B which has five higher frequency channels (89–190 GHz) primarily for humidity sounding (surface to 200 hPa). AMSU-A has a nominal field of view of 3.3° (45 km on surface at nadir) and AMSU-B a field of view of 1.1° (15 km on surface at nadir). AMSU-

A and AMSU-B sample 30 and 90 Earth views respectively, covering ±48.95° from the sub-satellite point.

The U.K. Meteorological Office (UKMO) is providing three AMSU-B flight instruments for the NOAA's K, L, and M polar orbiting satellites through a co-operative agreement with NOAA. Before launch the instruments are being comprehensively tested to determine their actual antenna, spectral, thermal and radiometric characteristics. This paper describes the radiometric tests which were carried out by the UKMO and the manufacturer British Aerospace Space Systems Ltd (BAe) and presents the results for the first flight model (PFM).

II. FUNCTIONAL DESCRIPTION OF AMSU-B

AMSU-B is a five-channel total power microwave radiometer with two channels nominally centered at 89 and 150 GHz and three centered on the 183.31 GHz water vapor line at 183.31 ± 1, ±3, and ±7 GHz. More details of the spectral characteristics of AMSU-B are given in Table I. The exact values of the central frequencies for each channel and their variation with instrument temperature in vacuum have been measured and are described in more detail elsewhere [2]. The passband sensitivity and limits have also been measured for each flight model [3]. The incident radiation is fed to three superheterodyne receivers via reflection from a single primary scanning antenna made of beryllium and from a secondary hyperboidal reflector and transmission through a quasioptical feed which splits the beam into the three required frequency bands using dichroic plates. Each receiver is operated in double sideband mode which helps to improve the sensitivity. For the 183.31-GHz receiver the IF is split into three bands which form channels 18–20. The IF signals are amplified and integrated for 18 ms and then digitized to 16-bit resolution.

Once every 2.667 s AMSU-B scans through 90 Earth views, four space views, and four internal black body target views. Note that there are also four possible viewing direction options for the space view, selectable by ground command, which view either closer to the limb of the Earth or closer to the spacecraft. During the commissioning phase of the spacecraft, investigations will be carried out to determine which of the four possible space view options give the lowest stable radiances and hence the most reliable calibration. The Earth viewing angles range from −48.95° to +48.95° about nadir and the sampling distance is 1.10°, giving a total of 90 Earth view samples. The nominal 3 dB beamwidth is equal to the sampling distance. The samples are numbered sequentially such that sample 1 is at the edge of the swath where the scan line starts and samples 45 and 46 are centered 0.55° either side of nadir. Measurements of the antenna pattern of the AMSU-B flight models have verified that the beamwidths are 1.1°
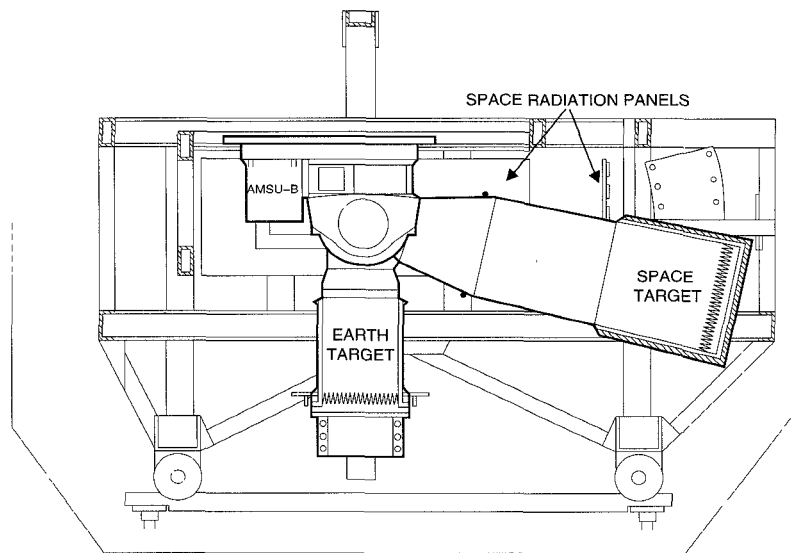
Fig. 1. The U.K. Met. Office facility for thermal and radiometric testing of AMSU-B.

TABLE I
NOMINAL CENTER FREQUENCIES, PASSBANDS,
AND POLARIZATION ANGLES FOR AMSU-B

Channel number designation	Centre Frequency of channel (GHz)	No. of Pass Bands	Channel Passband Limits		Polarization Angle[†]
			Lower GHz	Upper GHz	
16	89.0	2	87.6–88.6	89.4–90.4	90 − θ
17	150.0	2	148.6–149.6	150.4–151.4	90 − θ
18	183.31±1.00	2	182.06–182.56	184.06–184 56	90 − θ
19	183.31±3.00	2	179.81–180.81	185.81–186.81	90 − θ
20	183.31±7.00	2	175.31–177.31	189.31–191.31	90 − θ

† The polarization angle is defined as the angle from horizontal polarization, θ is the scan angle from nadir.

±0.11° as described in [4]. The scanning and sampling is designed such that 9 AMSU-B footprints are equivalent to one AMSU-A footprint. The four space views and internal target views during each scan are separated by 1° steps. The antenna rotation is not uniform, it accelerates and decelerates between the Earth views, space views and internal target views to increase the dwell time for the Earth and calibration views.

The polarization for all five channels is specified in Table I. AMSU-B is only sensitive to vertical polarization at nadir, where "vertical" polarization is defined for any scan angle as the polarization for which the electric field vector is perpendicular to the direction of satellite motion. However as the antenna rotates the ratio of horizontal to vertical polarization increases in direct proportion to the scan angle so that if the antenna could view at 90° to nadir only horizontally polarized radiation would be detected (i.e., electric field vector parallel to direction of motion). The polarization angle and sensitivity to cross-polarization are measured during the antenna tests.

The internal calibration target is comprised of a magnesium alloy substrate with pyramidal tines (aspect ratio 4:1) covered by a 1.3 mm layer of Eccosorb CR114. There are 7 two wire Platinum Resistance Thermometers (PRT's) in the internal target to monitor its temperature. The emissivity of a similar target has been radiometrically measured to be >0.9 999 [5]. The temperature of the internal target is passively controlled.

It is located in a particularly benign thermal environment and is well isolated against thermal instabilities and gradients, facilitated by a large thermal inertia. It is predicted to be around 20°C in orbit.

III. THE U.K. MET. OFFICE CALIBRATION FACILITY

The calibration facility is located on the U.K. Defence Research Agency (DRA) Farnborough site and allows the radiometric testing of AMSU-B to be performed under the full range of operating conditions using an existing 3-m thermal vacuum chamber. This allows a vacuum to be maintained to better than 10^{-5} torr. The facility is also used to temperature cycle the instrument in vacuum to qualify it before launch. The temperature of AMSU-B is controlled by space radiation panels held at 80 K on all sides of the instrument except in the Earth and Sun directions where a shroud is maintained at any desired temperature between 233 and 343 K. Heaters between the space radiation panels and the instrument also allow additional control of the instrument temperature. AMSU-B, the external calibration targets and the radiators are all mounted on a self supporting rig that can be removed from the chamber for ease of maintenance and alignment. A schematic diagram of the facility is shown in Fig. 1.

The 90 possible Earth views for AMSU-B are simulated by a movable black body target, hereafter referred to as the "Earth target," which for most of the tests is placed in a nadir view (taken as sample 46), but can be moved to be in any desired Earth viewing direction and in addition it can be placed in front of the space target. It is carefully temperature controlled over the range 80–330 K so that temperature gradients across the surface are less than 50 mK. The Earth target must also remain at a stable temperature (< 50 mK variation) for longer than 5 min (110 scans) and in practice it remains stable for much longer than this. The Earth target temperature is measured to an absolute accuracy of better than 0.1 K by regularly calibrating the PRT's with a "standard" PRT traceable to a national standard. A cylindrical "shroud" surrounds the target

which is maintained at a temperature as close to the target as possible (always within 1 K) and a "snout" (with reflective interior) closely couples the target to the antenna. A similar black body target is used for the space view, hereafter referred to as the "space target." This target is maintained at around 84 K for all the tests. This obviously gives a much higher space view radiance than experienced in orbit (i.e., 2.73 K) and so the instrument performance in space has to be extrapolated from these measurements.

Both targets are fabricated from aluminum substrates with pyramidal tines (aspect ratio 4:1) and coated with Eccosorb. The Earth target is closer (∼65 cm) to the instrument than the space target (∼135 cm), to allow it to be moved in front of the space target, and so is smaller (29.5 cm diameter) than the space target (40 cm diameter). Considerable efforts were made to ensure an accurate calibration for the external target PRT's as outlined in more detail in [6].

To determine a representative target temperature the five precision PRT's are averaged together in a manner to best represent the proportion of the target that the antenna "sees." For the tests described here the mean Earth and Space target temperatures are defined as

$$\bar{T}_{\text{targ}} = \frac{\sum_{i=1}^{5} w_i T_i}{\sum_{i=1}^{5} w_i} \quad \text{K} \tag{1}$$

the weights, w_i, being 1 for the center PRT and 0.5 for the four edge PRT's.

A check was made to see if the temperature of the shroud surrounding the Earth target affected the measured brightness temperatures. For warm target temperatures (i.e., 293 K) if the shroud was 5 K warmer or colder than the target then the brightness temperature for all AMSU-B channels was increased/decreased by 0.2 K. Model results show that this effect is consistent with radiative heating/cooling of the Eccosorb surface on the target by the shroud. The shroud temperature for the tests described below was always within 1 K of the target temperature and so the shroud should not significantly influence the measured brightness temperatures. An investigation of the effect of heating and cooling the space target shroud by 5 K above/below the target temperature showed no effect on the measured brightness temperatures as the infrared heating/cooling effect is much less at these temperatures. Therefore it was only required to be maintained to within 2 K of the target temperature.

IV. AMSU-B CALIBRATION

AMSU-B has been designed to allow a two point calibration, for each scan line, from the internal target and space views. The instrument response is assumed to be linear between these two calibration points. This allows the radiance from the antenna to be given by

$$R_{\text{Earth}}(i) = a(i) \times (C_{\text{Earth}}(i) - C_0(i)) \tag{2}$$

where $C_{\text{Earth}}(i)$ is the measured count (proportional to the receiver output voltage averaged over the scene integration time of 18 ms) for channel i while viewing the Earth scene.

TABLE II
THE BAND CORRECTION COEFFICIENTS FOR THE AMSU-B CHANNELS

Channel number	b	c
16	0.0	1.0
17	0.0	1.0
18	0 0	1.0
19	−0.0031	1.00027
19	−0.0167	1.00145

Calibration parameters (slope $a(i)$ and offset $C_0(i)$) are determined for every scan line from the internal target and space view counts. Equation 2 is written in this form because $C_0(i)$ is then directly related to receiver noise. The radiance unit assumed throughout is $\mu\text{W} \cdot (\text{cm}^{-1} \cdot \text{ster} \cdot \text{m}^2)^{-1}$ which was chosen as it scales to convenient values at these frequencies. The slope $a(i)$ (the reciprocal of the instrument gain) for channel i is given by:

$$a(i) = \frac{B(\nu, T'_{\text{BB}}) - B(\nu, T_{\text{SP}})}{(\bar{C}_{\text{BB}}(i) - \bar{C}_{\text{SP}}(i))} \tag{3}$$

where $B(\nu, T)$ is the Planck function for a frequency ν corresponding to the channel central frequency and temperature T. The subscripts BB and SP refer to the internal calibration blackbody target and the space view respectively. $a(i)$ has units of radiance/count. The Planck function uses the updated Planck constant and Boltzmann constant values given in [7]. The mean internal target temperature, T_{BB}, is computed from the 7 individual PRT temperatures

$$T_{\text{BB}} = \frac{\sum_{k=1}^{7} w_k \times T_k}{\sum_{k=1}^{7} w_k} + \Delta T_B \quad \text{K} \tag{4}$$

where the weights w_k are 0 or 1 in this case to exclude bad PRT's from the average (for all flight models PRT 6 was found to be consistently biased high and so was excluded from the average). ΔT_B is a correction factor assumed to be zero for all channels for these tests but could be used for the in-orbit data if a warm target bias is found (e.g., if the calibration of the PRT's was in error).

For channels 19 and 20 of AMSU-B the monochromatic assumption breaks down (e.g., channel 20 spans 16 GHz leading to errors of 0.4 K if a frequency of 183.31 GHz is assumed) and so band correction coefficients have to be applied, as is necessary for the HIRS infrared channels. These coefficients modify T_{BB} to give an effective temperature T'_{BB}

$$T'_{\text{BB}} = b + c \times T_{\text{BB}} \quad \text{K} \tag{5}$$

which is then used in the Planck function in (3) to give an accurate radiance. The values of the coefficients, b and c, are given in Table II.

For the radiometric tests in the chamber the space view has to be simulated by a cold target placed in the space view. T_{SP} is then the mean temperature of the space target (which is also converted to effective temperature for channels 19 and 20 using (5)). $\bar{C}_{\text{BB}}(i)$ and $\bar{C}_{\text{SP}}(i)$ are mean internal target and space view counts respectively. The means are computed from the four consecutive samples which view the internal target and space view for each scan line. In addition values from scan lines before and after the current scan line can also be included in the average. A triangular weighting function is convolved

with the mean space view counts, $\bar{C}_{\mathrm{SP}}(t)$, and internal target counts, $\bar{C}_{\mathrm{BB}}(t)$, for each scan line. This averages up to n scan lines ahead of and behind the current scan line, giving less weight to the lines further from the current scan line. For instance this convolution for the internal target counts can be written as

$$\bar{C}_{\mathrm{BB}} = \frac{1}{n+1} \sum_{j=-n}^{+n} \left(1 - \frac{|j|}{n+1}\right) \bar{C}_{\mathrm{BB}}(t_j) \quad \text{counts} \quad (6)$$

where t_j is the time of the scan line before or after the current scan line, that is $t_j = t + j \times 8/3$ s.

The zero radiance offset, $C_0(i)$, for channel i is given by

$$C_0(i) = \bar{C}_{\mathrm{BB}}(i) - \frac{B(\nu, T'_{\mathrm{BB}})}{a(i)} \quad \text{counts.} \quad (7)$$

$C_0(i)$ is related to the receiver noise (see below) and the dc offset applied to the video amplifier.

The radiance computed from (2), $R_{\mathrm{Earth}}(i)$, can be converted into effective brightness temperature using the inverse Planck function $B^{-1}(\nu, R_{\mathrm{Earth}})$

$$T'_{\mathrm{Earth}}(i) = B^{-1}(\nu, R_{\mathrm{Earth}}(i)) \quad \text{K.} \quad (8)$$

The actual scene brightness temperature, $T_{\mathrm{Earth}}(i)$, is then computed using the inverse of (5). Note that $T_{\mathrm{Earth}}(i)$ is strictly the antenna temperature which hereafter is referred to as brightness temperature. For ease of interpretation the results of the radiometric tests described below are all presented in terms of brightness temperature, as for scenes above 10 K brightness temperature is linearly related to radiance at these frequencies. All the calculations however were in terms of radiance as described above.

V. RADIOMETRIC TESTS

A series of tests were performed in the UKMO thermal vacuum chamber to fully characterize the radiometric response of the instrument. Most of the tests were carried out at several instrument operating temperatures to characterize the instrument behavior over the range of temperatures expected in orbit. For the purposes of these tests the "instrument temperature" was defined as the channel 18/19/20 mixer temperature which is available in the spacecraft telemetry and can be used to define the instrument temperature in-orbit. It was found that this temperature closely followed the mean receiver temperature determined from several thermocouples placed near all three receivers on the engineering model (EM). A full set of measurements were made at instrument temperatures of about 16, 26, and 36°C, which represent the minimum, nominal and maximum instrument temperatures expected in orbit. In addition a few radiometric checks were made at extreme instrument temperatures of 6 and 46°C to extend the measurement range of any temperature dependent parameters.

A. Temperature Sensitivity

The temperature sensitivity or noise equivalent temperature (NeΔT) of each channel of AMSU-B is a measure of the

TABLE III
RADIOMETRIC SENSITIVITY VALUES FOR THE AMSU-B PFM (STANDARD DEVIATIONS TAKEN OVER 100 SAMPLES WHILE VIEWING A 300 K TARGET)

Channel	Spec	Instrument Temperature					Measurement Uncertainty[†]
		6°C	16°C	26°C	36°C	46°C	
16	1.0K	0.35K	0.35K	0.37K	0.39K	0.39K	0.01K
17	1.0K	0.79K	0.76K	0.84K	0.78K	0.85K	0.02K
18	1.1K	0.99K	0.98K	1.06K	1 22K	1.26K	0.02K
19	1.0K	0.64K	0.68K	0.70K	0.80K	0.81K	0.02K
20	1.2K	0.53K	0.55K	0.60K	0.64K	0.76K	0.01K

† The 6°C and 46°C measurements have double these values.

minimum change in antenna temperature detectable by the receiver and is primarily a function of the input system noise T_{sys}. Other factors such as noise generated by the electronics, short term variations in gain and noise in the measured calibration counts also influence the sensitivity. A complete analysis is given in [8] but the following briefly summarizes the main factors which influence the sensitivity of a total power radiometer

$$\mathrm{Ne}\Delta T = T_{\mathrm{sys}} \left[\frac{1}{B_p \tau_s} + \frac{\sum_{j=-n}^{+n} w_j^2(t + jt_c)}{B_p \tau_c} + \left(\frac{\Delta G}{G}\right)^2\right]^{\frac{1}{2}} \quad (9)$$

where the first term is the receiver random noise for the scene, the second term is the receiver noise from the calibration views with a suitable weighted averaging applied to include data from adjacent scan lines (e.g., (6)) and the third term represents the nonuniform $1/f$ fluctuations in gain, G, described in more detail in the next section. B_p is the bandwidth and τ_s and τ_c are the integration times for the Earth and calibration views and t_c is the time interval between successive calibrations.

The sensitivity measurement is performed with the instrument at a stable temperature and the antenna scanning. With the Earth target at a temperature close to 300 K, 100 scans ($\sim$4.4 min) of nadir Earth target counts (i.e., sample 46) are extracted, converted into brightness temperature (as described above) and the standard deviation of the 100 brightness temperatures computed. Ten such runs are performed and the standard deviation values from each run are averaged to give the sensitivity value for each channel. In addition to determining the standard deviation for each channel the correlations between all the channels are also computed. It is important to know the channel covariances, if they are significant, when the radiances are used in a retrieval scheme [9]. For the results presented here the calibration parameters were all averaged over seven scan lines (i.e., $n = 3$) using (6).

The NeΔT results for the PFM at several instrument temperatures are listed in Table III, which also gives the specification for AMSU-B. Note however the specification only applies for instrument temperatures between 16 and 36°C. The only channel which is marginal is channel 18 where at least for warmer instrument temperatures the NeΔT values are above the required value. The correlation matrix which was computed for the five channels confirmed that they are uncorrelated.

Fig. 2 shows how the NeΔT values are reduced by about 0.1 K when the number of scan lines included in the weighted average of the calibration parameters is increased from 1 up to 7. Beyond this, the low frequency ($>$20 s) $1/f$ noise starts
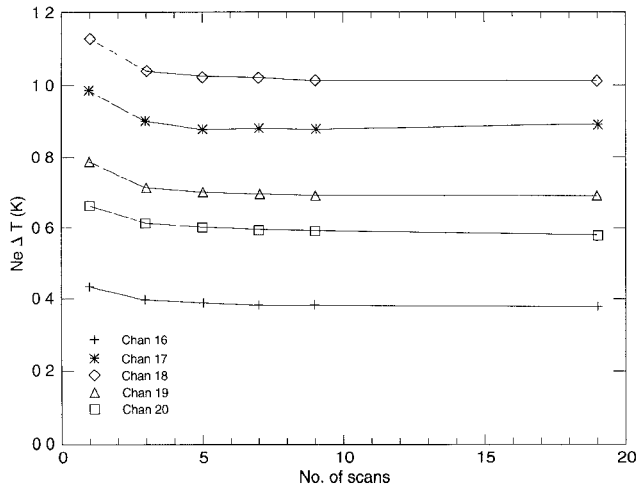
Fig. 2. The variation of NeΔT with number of scan lines included in the average of the space view and internal target counts for the PFM.
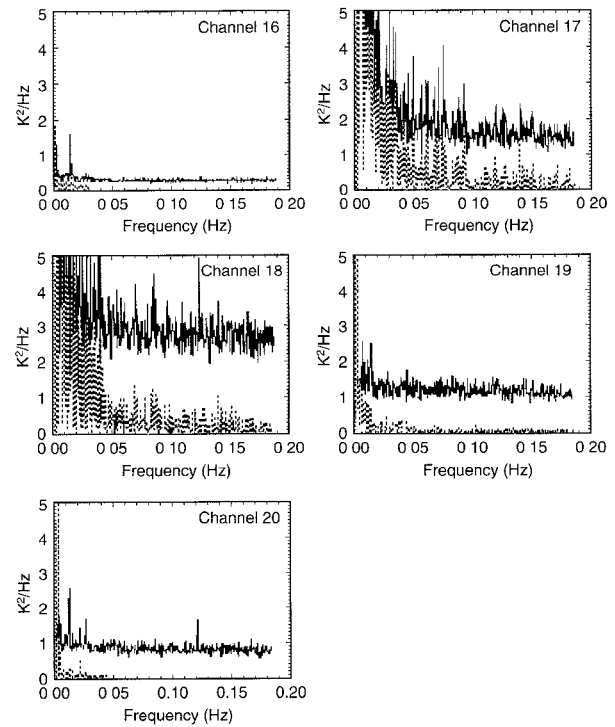

Fig. 3. The average power spectra for channels 16–20 with the antenna parked viewing the internal target for the PFM. The solid lines are spectra produced by averaging the 90 power spectra while the dotted lines are spectra produced by averaging the 90 samples for each scan before applying the FFT. The Nyquist frequency is at 0.1875 Hz.

to influence the means and the NeΔT starts to rise again. An optimum value for n in (6) appears to be 2 or 3 (i.e., 5 or 7 scan lines) for AMSU-B. NOAA and UKMO have agreed that a value of 3 be adopted in the operational processing for both AMSU-A and AMSU-B.

Once in orbit the NeΔT values will not be able to be measured directly but the variance of the internal target radiances will provide a measure of the noise for each channel. For the test data, with a value for n of 3, the internal target standard deviation values were typically 90% of the true values given in Table III. This is because the first two terms in (9) become correlated for the internal target views reducing the measured NeΔT values. Simulations with random noise give a ratio of 94% which is higher than the measured ratio due to the real noise having components of lower frequency variability.

B. Power Spectrum

To further quantify AMSU-B's low frequency receiver noise characteristics a power spectrum of the radiometer's output, while viewing a thermally stable target, is required. Note that "power" in this context refers to the radiometer output power, i.e., the square of the output voltage, not to radiant power, which is proportional to output voltage. High frequencies are dominated by white noise, with a uniform power spectral density. In this regime, the noise on the calibration parameters (a and C_0, defined in Section IV) will decrease as the number of calibration data samples averaged increases. For a uniformly weighted average, the noise would be inversely proportional to the square root of the number of scans averaged. Lower frequencies are dominated by $1/f$ noise, with a power spectral density increasing rapidly as the frequency decreases, and hence the calibration noise will start to increase as the number of scans averaged exceeds a certain limit. The frequency at which the $1/f$ noise starts to dominate the white noise is known as the "$1/f$ knee frequency," f_K.

For this test the antenna was parked viewing either the internal target or the Earth target, which were both maintained in a thermally stable environment at about 300 K for periods

>1 h. Power spectra were calculated using Fast Fourier Transform (FFT) routines on the radiometric data.

Consecutive Earth views are separated by 19 ms, so the 90 Earth views are sampled at a rate of 1/19 ms = 53 Hz. However, sampling at this rate is not continuous; there are breaks between Earth, space and internal target views. To achieve the regular sampling required for Fourier analysis it is necessary to take one FFT sample point per scan period (8/3 s). In the results to be presented in this section, two different methods are used to obtain these FFT sample points. In the first method, a separate FFT is done for each Earth view, resulting in 90 FFT's. The 90 power spectra are then averaged to reduce random variations. In the second method, the 90 Earth view data points are first averaged for each scan, then the averaged values are used as input for the FFT.

Fig. 3 shows spectra based on 1024 "scans," measured with the instrument at 26°C and the antenna parked viewing the internal target. The solid lines are spectra produced by the first method described above (the average of 90 power spectra) while the dotted lines are produced by the second method (the 90 samples are averaged for each scan before applying the FFT). The differences between the two curves can be explained by considering alias.

Each Earth view sample point is the integration of the receiver output signal over a period $\tau = 18$ ms. Such an integrator will attenuate high frequencies but pass low frequencies; quantitatively, the frequency response in power units will be the square of the Fourier Transform of a uniform window in the time domain, i.e., $G(f)^2$ where $G(f) = \sin(\pi\tau f)/(\pi\tau f)$.

The first null in the frequency response occurs at $f = 1/\tau = 55.6$ Hz; however the "ripples" in the $\sin(x)/x$ function extend to considerably higher frequencies. For a given time between samples, t, the Nyquist frequency (i.e., the highest frequency that can be represented by the sampled data) is given by $f_N = 1/(2t)$. Any frequencies higher than this will be aliased to lower frequencies, with attenuation given by $G(f)^2$.

For a white noise signal, the ratio of the "true" integrated power, P, between $f = 0$ and $f = f_N$ to the measured integrated power, P_M, (i.e., including alias) is given by

$$\frac{P}{P_M} = \frac{\int_0^{f_N} G(f)^2 df}{\int_0^{\infty} G(f)^2 df}. \tag{10}$$

If we take a single sample every 8/3 s, then $f_N = 0.1875$ Hz. Integration of $G(f)^2$ (with $\tau = 18$ ms) gives $P/P_M = 0.0067$, so most of the apparent white noise plotted in the solid lines of Fig. 3 is alias. Nevertheless, this situation corresponds fairly closely to the way the space view and internal target view data are actually used, except that in these cases 4 consecutive views are averaged, decreasing the width of the $\sin(x)/x$ function and hence reducing the alias contribution by a factor of approximately 4.

In the case where the Earth views are averaged prior to the FFT, each FFT sample point consists of a sequence of 90 18-ms windows, with 1-ms gaps between the windows. The frequency response of this function closely approximates to that of a uniform time-domain window with duration $\tau = 90 \times 19$ ms (except for frequencies close to $1/19$ ms $= 53$ Hz). The first null in $G(f)$ occurs at 0.58 Hz and the resulting value of P/P_M is 0.58. Thus there is still appreciable alias but it no longer dominates the signal. This method of data analysis is more relevant to the "true" spectral response of the instrument. In principle, the "true" (alias free) spectral response of the instrument might be obtained by filtering the time series prior to re-sampling, to attenuate frequencies above Nyquist. However, in practice such an approach is not possible because the receiver output is not recorded during the transitions between Earth, space, and internal target views (occupying approximately 44% of the total scan period). Note also that from the point of view of predicting the noise on the calibration parameters, inclusion of the appropriate amount of detector-noise alias is actually desirable.

The power spectra plotted in Fig. 3 show no anomalies except for a peak in channels 18 and 20 at 0.125 Hz (8 s) and in channels 16 and 20 at 0.015 Hz (69 s). The fact that the 0.125 Hz peak is much diminished when averaging 90 pixels is evidence that it is an alias of a higher frequency, probably 50 Hz.

The spectra used in this definition are those calculated from samples averaged over 4 consecutive views in the same way as the calibration data but with no averaging of adjacent scan lines. A best fit curve is calculated from the two components; white noise, with a slope of zero, and $1/f$ noise whose slope is calculated. The intercept of these components defines f_K.

Periods of 1024 scans were taken when the instrument temperature was stable at 6, 26, 36, and 46°C scanning across an Earth target held at a constant temperature of around 300 K.

Channel	f_K^{-1} secs
16	108
17	34
18	64
19	144
20	203

These tests showed no consistent changes in spectra with instrument operating temperature. The spectra were compared to those for a smaller number of scans, but again showed no consistent change. A check that the method was unaffected by target temperature was made by comparing spectra taken viewing the Earth target at 82 and 300 K. Again, there was no significant change in values of f_K. The f_K values from the tests were consistent with the results when the antenna parked was scanning.

The values presented in Table IV are the reciprocals of f_K averaged from all the above tests done on the PFM. They are related to the maximum time calibration parameters can be averaged over, before $1/f$ noise starts to increase the error in the average. It can be seen that the lowest value of $1/f_K$ is 34 s (13 scan lines) for channel 17. This is consistent with the small increase in channel 17 NeΔT values after averaging 19 scan lines, shown in Fig. 2.

C. Receiver Linearity

As implied by (3), a two point calibration is employed for AMSU-B (i.e., space and internal target). For all scenes with radiances in between these two calibration points it is assumed that the instrument response is linear. To determine to what level this assumption holds the Earth target was placed in the nadir view and radiance measurements were made for Earth target temperatures ranging from 85 to 330 K (with the space target at $\sim$84 K). This encompasses the full range of Earth scene temperatures but leaves the range from 2.7 to 85 K unmeasured. Ideally knowledge of linearity over this range is necessary when the instrument is operating in orbit in order to correctly relate the space view measured counts to radiance. The linearity of the individual electronic components has been measured at unit level for input signals corresponding to near zero radiance and their response was found to be linear. The increased difficulty of maintaining a target at 2.7 K *and* making target temperature measurements which are representative of the radiating surface ruled out this option in the vacuum chamber.

The measurements of linearity were made with the antenna in normal scan mode at three instrument temperatures 16, 26, and 36°C. The linearity measurements at instrument temperatures of 16 and 36°C were done with the Earth target temperature incremented in steps of 25 K between 85 and 330 K and the 26°C set of measurements were done with 15 K increments. The instrument temperature was required to vary by less than 0.1 K during these measurements. The space target temperature was kept roughly constant at around 84 K throughout. For each Earth target temperature at least ten 100 scan line "runs" were made during which the temperatures of
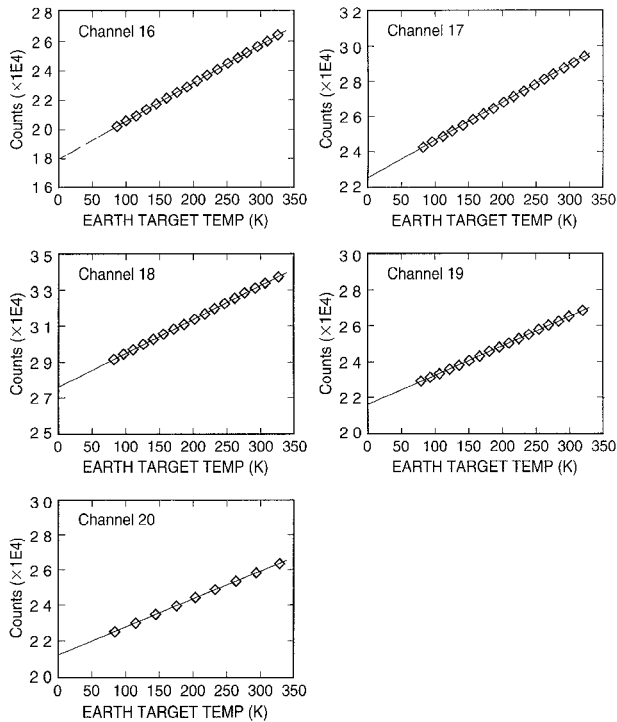
Fig. 4. Plots of counts for each channel as a function of Earth target temperature measured by the PRT's for the PFM.
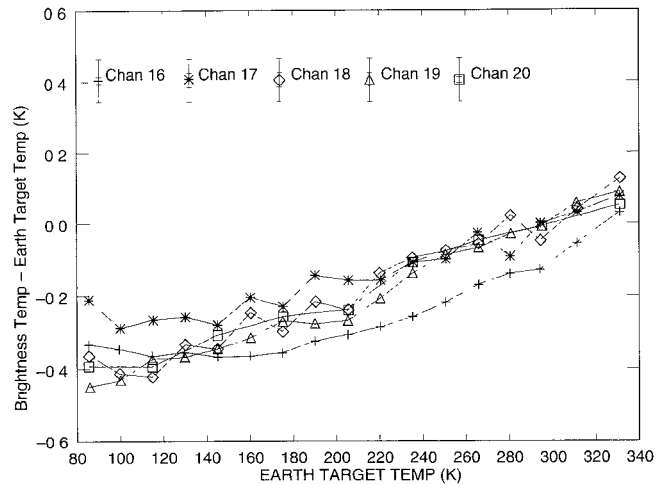

Fig. 5. Difference between measured brightness temperature of the Earth target and the measured target temperatures over the full range of target temperatures for an instrument temperature of 26°C and a nadir view. The relative and absolute uncertainties are shown by the smaller and larger error bars along the top for each channel.

both external targets were required to vary by less than 0.05 K and the gradients across the Earth and space targets to be less than 0.1 K.

Fig. 4 shows for the PFM the relationship between nadir view counts and Earth target temperature for all five channels for an instrument temperature of 26°C. This plot demonstrates several aspects of the instrument performance. Firstly the instrument can be seen to have a stable gain over the full range of linearity measurements. Secondly the linear response for targets between 85 and 330 K in all five channels is a verification of the receiver's dynamic range. Thirdly when extrapolated to zero radiance the instrument counts (i.e., C_0) are positive for all five channels. Note that the points for channel 20 in Fig. 4(e) are from a reduced set of runs with fewer Earth target temperatures due to the data being taken at a different time.

If the counts are converted into brightness temperatures using the calibration procedure described above, the differences between the AMSU-B calculated brightness temperatures and the actual target temperatures computed from (1) can be calculated. These differences are plotted as a function of target temperature in Fig. 5. This plot demonstrates the absolute calibration accuracy (see below) as well as the linearity of the receiver. To show more clearly any departure from linearity, Fig. 6 shows the differences from linearity in terms of brightness temperature for all five channels. These plots were produced as follows. Firstly a best fit line is computed through all the points of target temperature versus calculated AMSU-B brightness temperature. The departure of the points from this straight line fit is then plotted as the ordinate in Fig. 6. The specification for AMSU-B is that the peak departure from linearity should not exceed $0.3 \times Ne\Delta T$ (i.e., 0.3 K for

channels 16, 17, and 19; 0.33 K for channel 18; and 0.36 K for channel 20). In fact the results for the PFM shown in Fig. 6 show peak deviations no greater than ±0.1 K. No evidence is seen of any significant changes with instrument temperature.

The channel 16 plot does suggest a quadratic fit might be appropriate for this channel due to the close resemblance to the inherent nonlinearity of square law detectors. The correction required is small but for precision climate datasets it would be desirable to remove any residual biases due to nonlinearity. Also note the correction is bigger for the in-orbit data because the calibration points are further apart. More analysis of the laboratory data is underway to determine the form and magnitude of the correction required to the in orbit data.

D. Absolute Calibration Accuracy

The absolute calibration accuracy is defined as the difference between the "measured" brightness temperature and the actual calculated brightness temperature of a target determined from PRT's on the target and a knowledge of the target emissivity. The bias can only be estimated with confidence for the internal target calibration point (i.e., the warm bias). The mean of all the uncorrupted 100 scan line averages of nadir view brightness temperatures, when the Earth target is at the same temperature as the internal target, allows the warm bias to be determined. The standard deviation of the 100 scan line averages, which is the randomly varying component of the bias, is also computed.

Table V gives typical bias values measured for the PFM for both a nadir (pixel 46) and edge of swath (pixel 3) view. An error analysis for the warm bias measurements has been carried out which suggests the absolute uncertainty in the Earth target temperature is ±0.07 K and the standard error in the mean AMSU-B brightness temperatures ranges from ±0.006 K for channel 16 to ±0.028 K for channels 18 and 20. The relative and absolute measurement uncertainties are plotted on Fig. 5 and the latter are up to ±0.075 K. Given these uncertainties
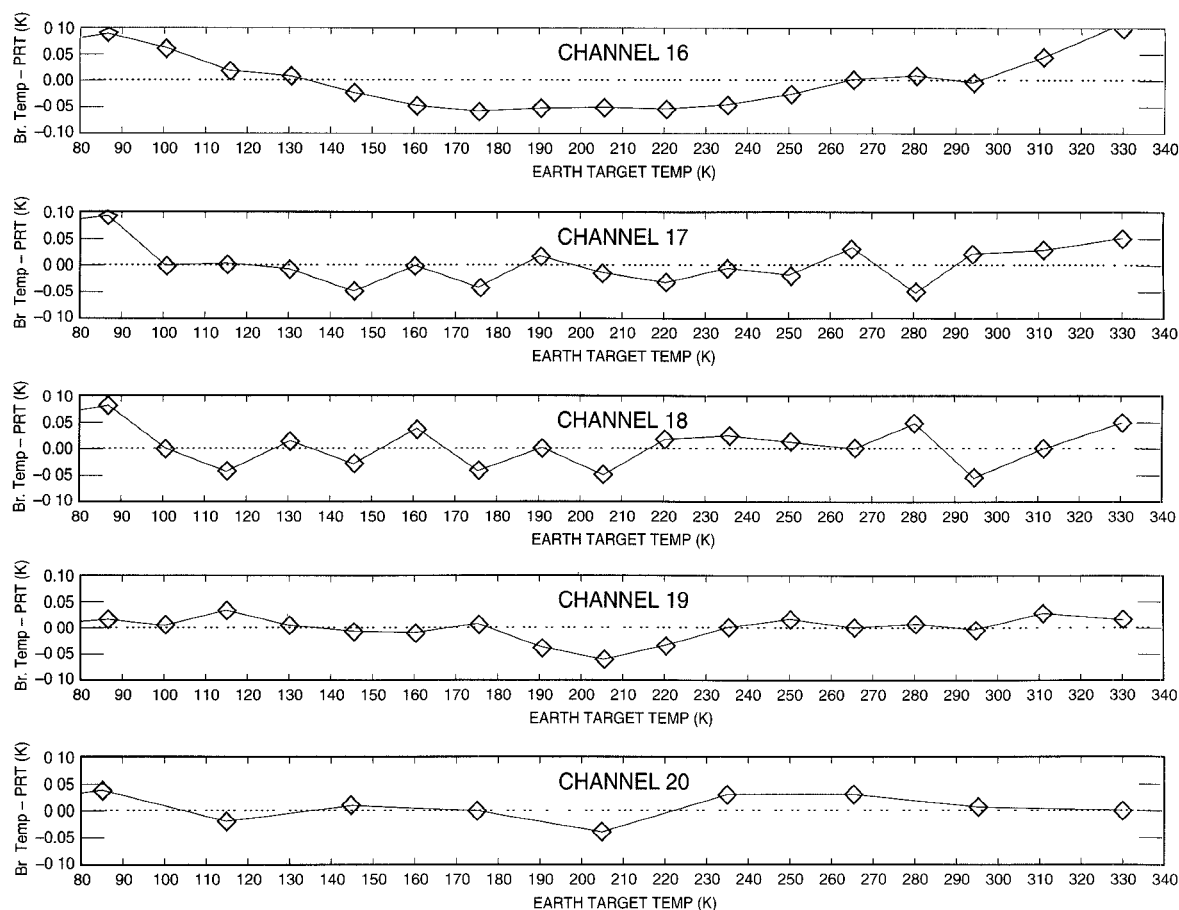
Fig. 6. Departure from linearity for the PFM at 26°C.

there is no significant warm bias measured except for channel 16 at nadir which is 0.12 K colder and channel 20 at pixel 3 which is 0.20 K warmer. The former may be caused by cooler stray radiation entering around the Earth target. The reason for the latter is not clear but further measurements have shown that the bias quickly reduces to zero as the nadir angle decreases and it is not evident on the opposite side of the scan. As the specification for AMSU-B is for the absolute calibration to be better than ±1 K for all channels the test results show the instrument is well within this criterion. The randomly varying part of the bias for the various channels listed in Table V ranged from 0.04 to 0.09 K. This is also well within the specification of 0.2 K for AMSU-B. Based on these measurements the correction factor ΔT_B in (4) for the PFM is taken to be zero for all channels and all views.

For the space view the best estimate of the bias in the absolute calibration which can be inferred in the laboratory is obtained from the measurements taken with the instrument viewing the Earth target at the same temperature as the Space target (i.e., ~85 K). In this case the error analysis must include the uncertainties in the measurement of the Space target temperature as this determines the channel gains and will not be present in the in-orbit configuration. Total uncertainties of ±0.10 K are estimated. At 85 K the mean biases measured at nadir range from −0.25 K for channel 17 to −0.47 K for channel 18. The cold biases are reduced for the view at the

TABLE V
MEAN AND RANDOM BIASES IN K FOR THE PFM DETERMINED BY VIEWING THE EARTH TARGET AT 300 AND 85 K. THE VALUES ARE COMPUTED FROM ELEVEN 110 SCAN LINE AVERAGES OF THE NADIR SAMPLE OVER A PERIOD OF 1 H. BOTH NADIR AND EDGE OF SWATH (I E, $\theta = 46.7°$) VALUES ARE INCLUDED THE VALUES IN BRACKETS BELOW ARE THE RESIDUAL BIASES AFTER THE SCAN DEPENDENT ADJUSTMENT HAS BEEN APPLIED

Channel	16		17		18		19		20	
View Angle	Nadir	Edge	Nadir	Edge	Nadir	Edge	Nadir	Edge	Nadir	Edge
Mean Bias measured at 300 K	−0.06	0.05	−0.01	0.10	0.06	0.06	0.03	0.05	0.0	0.20
	(−0.07)	(0.04)	(−0.02)	(0.09)	(0.05)	(0.05)	(0.02)	(0.04)	(0.0)	(0.20)
Mean Bias measured at 85 K	−0.25	−0.06	−0.27	−0.02	−0 47	−0.28	−0.43	−0.19	−0 39	0.02
	(0.18)	(0.16)	(0.16)	(0.20)	(−0.04)	(−0.06)	(0.0)	(0.03)	(0.05)	(0.24)
Random Bias required	<0.20		<0 20		<0 20		<0.20		<0 20	
Random Bias measured	0 04	0 05	0.08	0.07	0.09	0.07	0 08	0 08	0 06	0 07

edge of the swath. The values are listed in Table V. The random variations of the biases were the same as for the warm bias. The mean bias for the nadir view is plotted as a function of Earth target temperature in Fig. 5 over the full range of Earth target temperatures. The mean bias gradually decreases from typically −0.4 K at 85 K to zero at 293 K. The reason for the cold bias at the space view calibration point is believed to be due to a scan dependent variation in the gain of the instrument described in the next section.

All the warm biases measured remained the same over the full range of instrument temperatures (i.e., 6–46°C). The cold biases increased by typically 0.1 K between 6 and 46°C. This

is likely to be due to higher temperature radiation leaking into the space targets for the warmer instrument temperatures and is not an intrinsic property of the instrument. It should be borne in mind that for the in-orbit space view, problems of the antenna "seeing" the limb of the Earth and/or parts of the spacecraft will also need to be considered in the bias and so a correction factor $\Delta T_{SP}(\nu)$ will be required for the cold calibration point

$$T_{SP} = 2.73 + \Delta T_{SP}(\nu) \quad K \quad (11)$$

where $\Delta T_{SP}(\nu)$ is an estimate of the amount of radiation detected by AMSU-B in the space view in addition to the cosmic background at 2.73 K which has recently been measured at these frequencies [10]. $\Delta T_{SP}(\nu)$ will initially be pre-calculated for each channel and space view using a thermal model of the spacecraft and the measured antenna patterns. A rough calculation gives a value for ΔT_{SP} of 0.9 K for channel 16 [4]. The optimal values for ΔT_{SP} will need to be determined post-launch during the spacecraft commissioning phase.

E. Variation of Gains with Scan Angle

In order to investigate if the gain of AMSU-B varied with Earth viewing angle, the Earth target (at 100 K) was moved from its nominal nadir position to cover the full range of viewing angles (i.e., $\pm$ 48.95°). Bias measurements (i.e., mean brightness temperature minus Earth target temperature) were made with the Earth target positioned at several points between the two extremes of the scan and nadir. In addition the Earth target was also placed in space view 1 (67.6° from nadir) and space view 4 (79.7° from nadir) to further extend the range of angles measured on one side of the scan. The snouts which closely couple the instrument to the Earth and space targets had to be removed for this test which allowed more stray radiation to be incident on the antenna. Also for Earth target positions close to or in the space views (i.e., samples 62–90; beyond 17° from nadir) the Earth target starts to intrude into the space view. For these measurements the Earth target counts were measured for 5 min, followed by the space target counts, as the Earth target was moved out of the way. The space target counts were then used to define the space view calibration for the earlier Earth target measurements. The difference in time ($\sim$5 min) between the determination of the calibration coefficients and the bias measurements viewing the Earth target increased the uncertainties.

Fig. 7 shows the bias as a function of scan angle for the second flight model (FM2) with the Earth target at 100 K (the PFM plot was similar but the lower noise figures for FM2 led to a clearer plot). Firstly note that the overall biases are larger because of the additional stray radiation with no snouts present especially for channel 16 which has a lower beam efficiency [4]. More significantly there is also a clear reduction in the cold bias for scan angles well away from nadir. This was confirmed by doing a full linearity run with snouts on at Earth target position 3 (i.e., nadir angle of 46.7°). The cold biases were significantly reduced by up to 0.4 K as shown in Table V. The reason for this behavior is still being investigated but is thought to be an inherent property of the instrument.
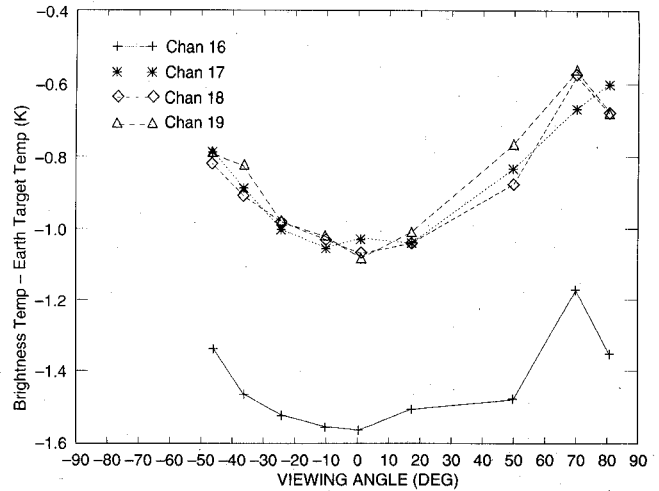

Fig. 7. The mean bias (measured brightness temperature minus Earth target temperature) as a function of scan angle with the Earth target temperature at 100 K for FM2.

The measurements shown in Fig. 7 can be used to derive an empirical radiance adjustment factor which varies with nadir viewing angle and scene temperature. A best fit to the data suggests a correction, $\Delta R(\nu)$ which is added to the measured radiance, of the form

$$\Delta R(\nu) = \gamma(\nu) \frac{(R_{BB}(\nu) - R_{Earth}(\nu))}{(R_{BB}(\nu) - R_{SP}(\nu))} \sin(75° - |\theta|) \quad (12)$$

where $\gamma(\nu)$ is the empirically determined scaling factor for each channel derived from the measured channel 19 cold bias at nadir, R_{BB}, R_{SP} and R_{Earth} are the radiances of the internal target, space view and Earth view respectively and θ is the angle from nadir. Channel 19 was chosen to define the cold bias as it has the highest beam efficiency and so the effects due to stray radiation will be minimized. The application of this correction to the measured Earth target radiance removes most of the cold biases for all scan positions as shown in Table V. The resultant positive biases for channels 16 and 17 are thought to be due to warmer stray radiation leaking into the targets only affecting the channels with lower beam efficiencies and so will not be present in orbit.

F. Variation of Calibration with Instrument Temperature and Time

During the duration of the characterization tests the gains/offsets were continuously monitored during six thermal profiles of the instrument between 6°C and 46°C. The gains (i.e., $1/a(i)$) and offsets (i.e., $C_0(i)$) of each channel for five instrument temperatures during the September 1993 tests on the PFM are plotted in Fig. 8.

The offsets, which are related to system noise temperature, for each channel (defined as $C_0(i)$ in (2)) do vary more significantly with instrument temperature as illustrated in the right-hand panel of Fig. 8. However the applicability of these data for in-orbit conditions may not be valid since the offset is also a function of the video amplifier temperature which may be subject to different thermal forcing in-orbit than in the
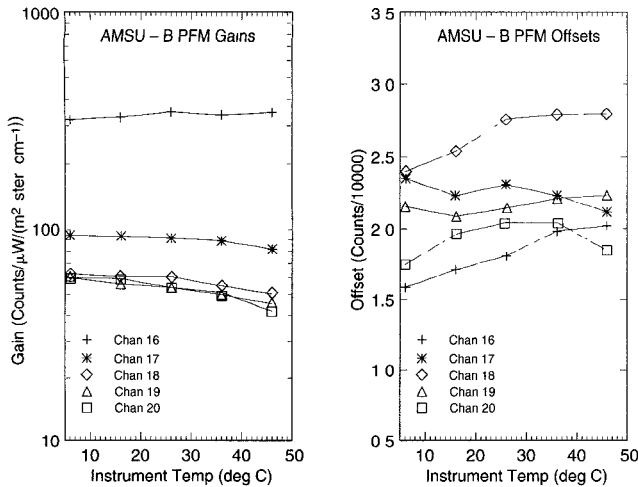
Fig. 8.   The measured variation of gain and offset as a function of instrument temperature for the PFM.

chamber. This means for a given instrument temperature the offset in orbit may vary significantly from the values plotted in Fig. 8. Evidence of this is seen in the orbital simulations described below where the thermal forcing is varying.

At the nominal instrument temperature of 26°C the gains all varied by less than 6% from the start to the end of the profiles. To monitor any temporal variations in the instrument gains and offsets before launch a program of tests has been devised to allow these parameters to be monitored regularly while the instrument is mounted on the NOAA spacecraft.

G. Simulation of Orbital Temperature Cycling

To simulate the variations in temperature that AMSU-B will experience around an orbit a test was carried out in the chamber where the instrument temperature was forced to vary in a similar manner to that predicted by a thermal model for orbital conditions. The thermal model itself has been verified by measuring the thermal behavior of the EM in a solar simulation chamber which was also able to simulate orbital conditions. The receiver temperature variations achieved were 0.8 K around an orbit which was 0.1 K greater than that predicted by the thermal model. However one simulated orbit took 2 h, whereas the real orbital period is 100 min. The PFM was subjected to ten orbital cycles.

As an example, the results for channel 17 of PFM are illustrated in Fig. 9. The top panel shows the temperature of the channel 17 mixer; note that the instrument was still warming up slightly for the first few cycles. The maximum amplitude of the mixer temperature variations was less than 1 K. The internal target temperature shown in the next panel was gradually warming up during the period from 21.5 to 23.5°C. It lags behind the receiver temperature as it has a large thermal inertia. The variation of the offset is shown in the next panel, the offset varies by about 1%, increasing with receiver temperature (with some time lag). The variation is inconsistent with the steady state relationship between offset and temperature, which shows a decrease in offset with increasing temperature (Fig. 8). This shows how sensitive the offset is to the thermal forcing applied to the instrument.

The effect on the gain is less, although a small (<0.4%) variation in gain around the orbit is evident. Finally the bottom two panels show the effect on the retrieved Earth target brightness temperatures, together with the actual Earth target temperature. The brightness temperatures have been averaged over 99 scan lines before plotting. There is no evidence of the orbital temperature variations influencing the measured brightness temperatures, and this was true for all channels. The bias of ∼0.2 K between the bottom two panels in Fig. 9 is consistent with the measured bias plotted in Fig. 5 for a 200 K Earth target. Note that despite the averaging the small ±0.1 K changes in target temperature toward the end of the period could not be detected.

VI. CONCLUSION

An extensive series of radiometric tests on the AMSU-B flight models has been successfully carried out in the UKMO test facility at Farnborough. The results show that the PFM is within or very close to specification in all aspects of its radiometric performance. The figures for the NeΔT of the 5 channels show that channels 16, 17, 19, and 20 are all below 1.0 K but channel 18 has a value of typically 1.1 K. The receiver has a linear response to within ±0.1 K for scene temperatures between 85 and 330 K obviating the need for a nonlinear correction factor (with the possible exception of channel 16). The absolute calibration of the instrument for nadir views shows no significant bias (i.e., <0.15 K) for the internal target calibration point and for the space target calibration point when a scan dependent correction is applied. Even before correction all the biases are well below the specification of 1.0 K. The changes in gain with instrument temperature are relatively small (<16% over the full range of temperatures expected in orbit). There is a small variation of gain with scan angle which could be corrected for to obtain the optimal calibrated radiance. Subjecting the instrument to the temperature variations expected in orbit did not affect the measured brightness temperatures. Before the launch of NOAA-K the gains, offsets and NeΔT figures for PFM will be routinely monitored to check there are no sudden changes in the instrument performance.

A final adjustment which could be applied is to correct for cold space beyond the limb of the Earth seen in the antenna sidelobes which reduces the measured Earth radiance. This effect is largest for Earth viewing angles at the edges of the swath. Calculations using the measured antenna patterns suggest in the worst case for channel 16 this effect reduces the brightness temperatures by 0.7 K [4].

The other two AMSU-B flight models (FM2 and FM3) both show characteristics similar to the PFM when under test in the vacuum-chamber. A technical report giving the same results for these flight models as those presented above for the PFM is in preparation and will be available from the UKMO. The AMSU-A engineering models have also been radiometrically tested in a thermal vacuum chamber [11]. It is planned to test the AMSU-A1 engineering model in the UKMO chamber which will provide an opportunity to cross-calibrate AMSU-A1 and AMSU-B. A technical document
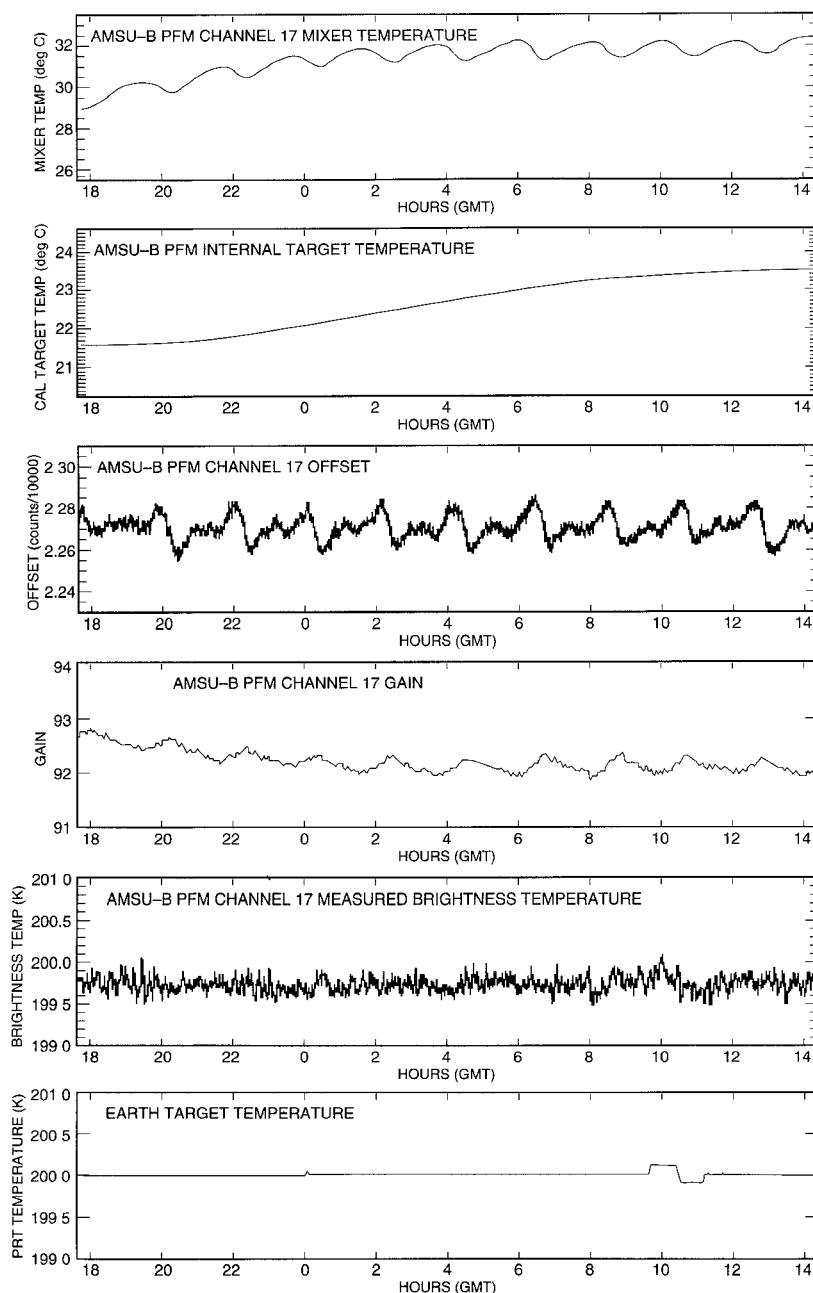
Fig. 9.   The variation of various parameters for channel 17 during the orbital cycling of the PFM.

describing the recommended calibration procedure for both AMSU-A and AMSU-B and giving the coefficients required, for each flight model, is in preparation by NOAA and UKMO.

Once AMSU-B is launched it is planned to monitor the in-orbit radiometric sensitivities and gains and to validate the data using global atmospheric model analyses and intensive field campaigns as is being carried out with current microwave radiometers [12]. The laboratory data will be valuable to aid interpretation of the in-orbit data.
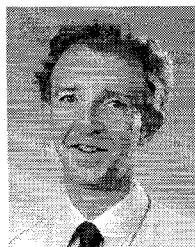
ACKNOWLEDGMENT

British Aerospace Space Systems Ltd is the prime contractor for building the AMSU-B and was closely involved in formu-

lating the radiometric tests to ensure the instrument met the specification. Aerojet ESD provided the receivers for AMSU-B. The efforts of both B. Greener's team in RSI (UKMO) and the DRA personnel are acknowledged in carrying out the tests in a timely fashion.

REFERENCES

[1] J. R. Eyre, "Information content from satellite sounding systems: A simulation study," Q. J. Roy. Meteor. Soc., vol. 116, pp. 401–434, 1990.
[2] T. J. Hewison, "Monitoring AMSU-B local oscillators," Remote Sensing Instrumentation, Hants, U.K., RSI Branch Working Paper no. 35, 1992.
[3] M. L. Jarrett and J. E. Charlton, "Characterisation of the channel passband response of AMSU-B," in Proc. Microwave Instrumentation for Remote Sensing of the Earth, SPIE, Orlando, FL, Apr. 13–14, 1993, pp. 169–177.
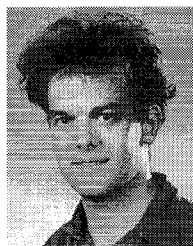
[4] T. J. Hewison, "AMSU-B antenna test results," in *Proc. Specialist Meeting on Microwave Radiometry and Remote Sensing of the Environment*, Rome, Italy, Feb. 14–17, 1994.

[5] ———, "Reflectivity tests of microwave black body targets," Remote Sensing Instrumentation, Hants, U.K., RSI Branch Working Paper no. 27, 1991.

[6] N. C. Atkinson and M. V. Ricketts, "Calibration of E109 PRT's, July 1992 to Apr. 1994," Remote Sensing Instrumentation, Hants, U.K., RSI Branch Working Paper no. 63, 1994.

[7] E. R. Cohen and B. N. Taylor, "The fundamental physical constants," *Physics Today*, pp. 9–13, Aug. 1992.

[8] M. S. Hersman and G. A. Poe, "Sensitivity of the total power radiometer with periodic absolute calibration," *IEEE Trans. Microwave Theory Tech.*, vol. MTT-29, pp. 32–40, Jan. 1981.

[9] C. D. Rodgers, "Retrieval of Atmospheric temperature and composition from remote measurements of thermal radiation," *Rev. Geophys. Space Phys.*, vol. 14, pp. 609–624, Nov. 1976.

[10] B. Schwarzschild, "COBE satellite finds no hint of excess in the cosmic microwave spectrum," *Physics Today*, pp. 17–20, Mar. 1990.

[11] T. Mo, M. P. Weinreb, N. C. Grody, and D. Q. Wark, "AMSU-A engineering model calibration," NOAA Tech. Rep. NESDIS 68, 1993.

[12] J. P. Hollinger, J. L. Peirce and G. A. Poe, "SSM/I instrument evaluation," *IEEE Trans. Geosci. Remote Sensing*, vol. 28, pp. 781–790, Sept. 1990.

Timothy J. Hewison received the B.Sc. (Hons.) degree in physics with astrophysics from the University of Manchester, U.K., in 1989.

Since 1990 he has worked in the Remote Sensing Instrumentation branch of the U.K. Met. Office. His work has included testing of the AMSU-B antennae, local oscillators, power spectra, and calibration targets and the development of a new microwave radiometer for the U.K. Met. Office C-130 research aircraft.
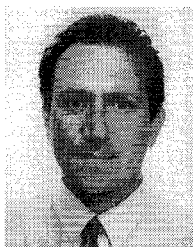
Stephen J. Stringer received the B.Sc. (Hons.) degree in physics and maths from Reading University in 1983 under sponsorship from the U.K. Met. Office.

From 1983 he has been with the Remote Sensing Instrumentation Branch of the U.K. Met. Office working with millimeter wave and infrared radiometers, concentrating mainly in the areas of calibration and test. Recent years have been devoted to the setting up of a facility, purpose built for performance and characterization testing of the AMSU-B. Work now progresses for wider application use of the facility. He has recently moved within the Met. Office to take up a new post as UKMO Data Licensing Manager.

Roger W. Saunders received the Ph.D. degree in 1980 from Imperial College, University of London.
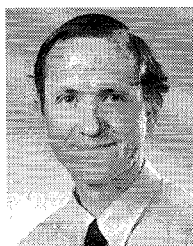
Since then he has worked in the field of satellite remote sensing at University College London, Rutherford Appleton Laboratories, U.K. and the European Space Operations Center at Darmstadt, Germany. He joined the U.K. Met. Office in 1984 and is now the AMSU-B project scientist. He heads a group responsible for addressing the scientific aspects of AMSU-B both from the instrumental viewpoint from the thermal-vac test results and improving our knowledge of the radiative transfer of the atmosphere at AMSU-B frequencies. To help in the latter aim two microwave radiometers are being flown on a research aircraft.

Nigel C. Atkinson received the B.A. (Hons.) degree in physics from Oxford University in 1982.

Since joining the U.K. Met. Office in 1982 he has worked on the development of various research and operational instruments, including ground-based, balloon, aircraft and satellite instruments. He is currently part of the team responsible for the testing of AMSU-B in thermal-vacuum. He is also involved in studies of signal-processing and alias reduction in future satellite-borne imagers and sounders, aimed at optimizing the instrument design to suit the intended meteorological applications.